NeuroImage xxx (2013) xxx–xxx

Contents lists available at SciVerse ScienceDirect

NeuroImage

journal homepage: www.elsevier.com/locate/ynimg

A segmentation protocol and MRI atlas of the C57BL/6J mouse neocortex

Jeremy F.P. Ullmann [b,*,1], Charles Watson [a,c,1], Andrew L. Janke [b,1], Nyoman D. Kurniawan [b], David C. Reutens [a,b]

[a] The Australian Mouse Brain Mapping Consortium, The University of Queensland, Brisbane, Australia
[b] Centre for Advanced Imaging, The University of Queensland, Brisbane, Australia
[c] Health Sciences, Curtin University, Bentley, Western Australia, Australia

ARTICLE INFO

Article history:
Accepted 5 April 2013
Available online xxxx

Keywords:
Atlas
Cortex
Isocortex
Magnetic resonance imaging
Segmentation

ABSTRACT

The neocortex is the largest component of the mammalian cerebral cortex. It integrates sensory inputs with experiences and memory to produce sophisticated responses to an organism's internal and external environment. While areal patterning of the mouse neocortex has been mapped using histological techniques, the neocortex has not been comprehensively segmented in magnetic resonance images. This study presents a method for systematic segmentation of the C57BL/6J mouse neocortex. We created a minimum deformation atlas, which was hierarchically segmented into 74 neocortical and cortical-related regions, making it the most detailed atlas of the mouse neocortex currently available. In addition, we provide mean volumes and relative intensities for each structure as well as a nomenclature comparison between the two most cited histological atlases of the mouse brain. This MR atlas is available for download, and it should enable researchers to perform automated segmentation in genetic models of cortical disorders.

Introduction

The neocortex is the largest component of the telencephalon in the mouse. The histology of neocortical areas, typically composed of six layers of neurons, distinguishes them from the olfactory cortical areas (which contain only three distinct layers) and from the hippocampal regions. Large areas of the mouse neocortex serve as primary receiving areas for somatosensory, visual, auditory, vestibular, taste, and visceral sensations. Cortical areas subserving motor function are also relatively large, and are located rostral to the somatosensory cortex. The remainder of the mouse neocortex comprises the orbitofrontal, the cingulate/retrosplenial, and the parietal association cortical areas.

Segmentation of the mouse neocortex is challenging, but there are obvious transitions between many of the functionally distinct regions. Taken together, the many histological and electrophysiological studies of mouse cortex over the past century reveal a clear picture of areal patterning (Kirkcaldie, 2012). These studies have been based on cytoarchitectonics (Caviness, 1975; Wree et al., 1983), chemoarchitectonics (Franklin and Paxinos, 2008; Hof et al., 2000; Watson and Paxinos, 2010), electrophysiology (Tennant et al., 2011), thalamocortical connections (Jones, 2007) cortical efferent connections (Larsen et al., 2007; Meltzer and Ryugo, 2006) and gene expression studies (Bohland et al., 2010; Hawrylycz et al., 2010; Ng et al., 2009). The most comprehensive modern maps of the C57BL mouse cortex are found in the stereotaxic atlases of Paxinos and Franklin (2013) and Dong (2008). The boundaries identified in these two atlases are very similar in all but a few instances. The present study makes extensive use of the maps in these two atlases.

The shape and size of the primary regions (such as the visual, auditory and somatosensory regions) in mouse neocortex can vary significantly across strains (Hof et al., 2000). For example, inter-strain variations have been found in total cortical volume (Gaglani et al., 2009), and there are more localized differences in the size of the barrel field (Jan et al., 2008; Li et al., 2005) and the visual cortex (Airey et al., 2005, 2006). More marked alterations to cortical morphometry and connectivity occur in natural mutants and transgenic models of neurological disorders such as Huntington's (Lerch et al., 2008a,b; Zhang et al., 2010) and Alzheimer's disease (Benveniste et al., 2007; Lau et al., 2008b).

Magnetic resonance imaging (MRI) has become an important technique for examining changes in brain structure in mouse models of neurological disorders (Benveniste et al., 2007; Lau et al., 2008b; Nieman et al., 2005; Pitiot et al., 2007). The combination of image registration methods and voxel-based statistical parametric mapping techniques has been used to identify phenotypic differences between disease and control animals (Lerch et al., 2008b; Sawiak et al., 2009). While comparisons at the cortical level can already be performed using established whole-brain mouse atlases, a detailed atlas of the C57BL/6J neocortex is needed to allow researchers to map the changes at a regional and functional level. Therefore, in this paper we present a detailed protocol for segmenting the C57BL/6J cortex using high-resolution MRI and a minimum deformation atlas made

* Corresponding author at: Centre for Advanced Imaging, The University of Queensland, Brisbane, QLD 4072 Australia. Fax: +61 7 3346 0330.
E-mail address: j.ullmann@uq.edu.au (J.F.P. Ullmann).
[1] Contributed equally to this work.

1053-8119/$ – see front matter © 2013 Published by Elsevier Inc.
http://dx.doi.org/10.1016/j.neuroimage.2013.04.008

up of averaged data from 18 individuals. This atlas is made freely available to assist future researchers in automatic segmentation of the mouse neocortex.

Materials and methods

C57BL/6J mouse brain preparation and magnetic resonance imaging

Eighteen animals (male, 12 week old) were perfused and fixed with 4% paraformaldehyde and 0.1% Magnevist® (gadopentetate dimeglumine, Bayer HealthCare Pharmaceuticals Inc., Wayne, NJ, USA) in phosphate buffer (PB). Brains were extracted and incubated in 0.1% Magnevist/PB for 4 days, placed in Fomblin (Solvay Solexis, Milan, Italy) and imaged on a 16.4 T (89 mm bore diameter) Bruker micro-imaging system (Bruker Biospin, Karlsruhe, Germany) using a 15 mm SAW coil (M2M Imaging, USA). MRI data were acquired using a 3D gradient echo sequence with a repetition time = 50 ms, echo time = 12 ms, flip angle = 30°, 82 KHz spectral bandwidth, field of view = 2.1 × 1.5 × 0.75 cm, matrix = 700 × 350 × 250, 8 averages, resulting in a total acquisition time of 5 h 15 min, to produce T_2*-weighted images at 30 μm isotropic resolution.

Minimum deformation atlas creation

Images were placed in the Waxholm stereotaxic coordinate space (Johnson et al., 2010) and a symmetric model was created using a recursive non-linear hierarchical fitting strategy similar to that employed by Fonov et al. (2011). The fitting strategy consisted of 3 linear fits to the evolving internal model followed by a hierarchical series of non-linear grid transforms. These transforms used progressively smaller millimeter step sizes of 1.067, 0.533, 0.267, 0.2, 0.133 and 0.06 mm. The fitting uses smoothed data with a 3D FWHM of half the step size. 20 iterations at each fitting stage were performed using the ANIMAL algorithm. Interpolation resulted in a model with 15 μm^3 isotropic voxels (Janke et al., 2012).

Our technique differs from Fonov et al.'s (2011) during the intermediate model generation in that a robust averaging process is used to reduce the effect of artifacts and small handling tears in the brain. The averaging technique places a lower weight on data at each voxel that is greater than 2 standard deviations from the current model. The fitting process took ~3 weeks on a 50core commodity Debian GNU/Linux cluster.

Segmentation

The major anatomical features of the neocortex were primarily identified on the coronal sections of the model by a single expert anatomist (CW) who is the co-author of a number of rodent brain atlases (e.g. Paxinos and Watson, 2007; Paxinos et al., 2009; Watson and Paxinos, 2010). The operational criteria for defining anatomical features were defined in terms of differences in signal intensity and/or their location with reference to anatomical landmarks. The cortex was segmented into major regions and subregions using the parcellation scheme of Paxinos and Franklin (2013). In some cases our parcellation was more conservative than in the atlas, and where anatomical landmarks or clear boundaries of sub-regions could not be defined, the areas were combined. Structures were then partitioned according to the operational criteria using vector-based segmentation performed on a Cintiq tablet (Wacom Company Ltd, Vancouver, USA). The complete data set was then exported to Amira (Visualization Sciences Group, Burlington, USA) where structural boundaries were checked and corrected in the three orthogonal planes by JFPU and CW. In total, segmentation required approximately 1000 h to complete. The nomenclature and abbreviations used here were taken from Paxinos and Franklin (2013) and the color palette for cortical structures is based on that used in the BrainNavigator (Elsevier Inc., Amsterdam, Netherlands) website. Finally, smoothed three-dimensional surface reconstructions were created in Amira. Average image intensities were computed by first normalizing the intensity values in the model to lie between 0 and 100 via percent critical thresholding of the intensity histogram for the entire image. In our case cutoffs of 0.1% and 99.9% were used. The signal intensity across the structures of interest was then averaged. Structure volumes were computed in model space from the delineated labels.

Results

The minimum deformation atlas represents the average spatial positioning and intensity of each structure. Fig. 1 demonstrates the superior signal and contrast to noise ratios in comparison to the image from a single brain, features which assisted the delineation of cortical structures. The improved clarity indicates quality of the registration.

Table 1 lists the structures, abbreviations according to Paxinos and Franklin (2013), their corresponding color, average volume, and average signal intensity. Where possible, the corresponding abbreviations of Dong (2008) are provided to enable correlations with gene expression and other data assembled by the Allen Brain Institute. Discrepancies between the two nomenclature systems are addressed in the Discussion.

Identification of anatomical boundaries

The key to segmentation of the isocortex is the ability to visualize the slight intensity differences that occur between the pattern of layers in different functional regions. Accurate segmentation requires significant expertise in MRI-based neuroanatomy and histological anatomy. Fig. 2 demonstrates the six cortical layers with the grayscale intensity corresponding to the neuronal and fiber tract density in the six layers. When directly comparing a section from the minimum deformation atlas with its corresponding section from The Allen Reference Atlas (Dong, 2008), the outer layer (a) is hyperintense and appears to correspond to Layer 1; the next darker lamina (b) to Layers 2/3, the superficial part of the lighter layer (c) to Layer 4 and a little of the deeper part to Layer 5; the next darker layer (d) to Layer 5; and finally the brighter lamina (e) to Layer 6. While the lamination can clearly be seen the layers were not segmented, as it was difficult to distinguish the laminae across the entire cortex.

The MR characteristics of the major cortical areas in the mouse can be appreciated by studying a spaced series of coronal sections that have been selected to show the different cortical regions to advantage.

The following sections have been selected for detailed consideration:

1. Fig. 3a shows a coronal section including the large motor regions of the frontal lobe (M1 and M2) and the rostral part of S1, along with the areas that form the medial wall of the frontal lobe.
2. Fig. 3b shows a section passing through the anterior commissure and is dominated by the large area occupied the somatosensory cortex (S1Br, S1FL and S1HL, and S2), with the motor and cingulate areas dorsomedially and the insular cortex ventrally.
3. Fig. 3c shows a section passing through the caudal part of the barrel field of the somatosensory cortex. The parietal association areas lying between the S1 trunk area and the retrosplenial cortex are seen. The section also shows the rostral part of the ectorhinal and perirhinal cortical areas between S2 and the piriform cortex.
4. Fig. 3d shows a section passing through the splenium (caudal end) of the corpus callosum and the caudal tip of S1. It includes the primary visual cortex (V1), the primary auditory cortex (Au1) and their respective association areas.
5. Fig. 3e shows a section passing through the caudal tip of the dentate gyrus, containing the center of the primary visual cortex (V1M and V1B), the visual association areas on either side of the

Please cite this article as: Ullmann, J.F.P., et al., A segmentation protocol and MRI atlas of the C57BL/6J mouse neocortex, NeuroImage (2013), http://dx.doi.org/10.1016/j.neuroimage.2013.04.008

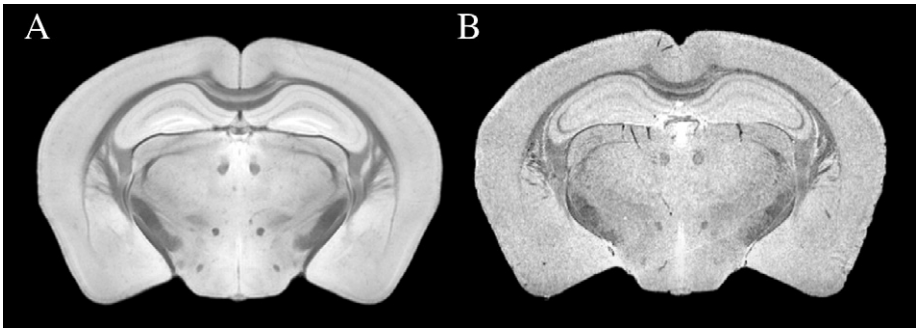

Fig. 1. Comparison of contrast and resolution between the minimum deformation model (A) made up of 18 brains and one individual (B). Note the decreased noise and artifacts present in the model.

primary auditory cortex (Au1) and their respective association areas.

Fig. 3a shows the large motor regions of the frontal lobe (M1 and M2) and the rostral part of S1, along with the areas that form the medial wall of the frontal lobe. The three large regions that form the superolateral surface in this section (M2, M1, S1) share a thick superficial dark band. They can be distinguished from each other by the appearance of the middle layer deep to the dark layer. In S1 this middle layer is much lighter than the adjacent M1. On the medial side of M1 the middle layer again becomes lighter in the M2 region. The transition from S1 to the insular cortical areas (Ins) is marked by an abrupt thinning of the superficial dark layer, the darkening of the middle layer, and the appearance of a thin dark band in superficial layer 5. The brighter superficial layer in the insular cortex fades out from dorsal to ventral as it approaches the border with the piriform cortex. The piriform cortex has a number of characteristic features — a light band in layer 1, a thin dark band marking layer 2, and brighter intensity in layer 3. On the dorsomedial wall of the frontal lobe, there is a gradual increase in overall intensity from dorsal (A24b) to ventral (DTT). A24b has a relatively hypointense superficial band, but this band is markedly less dark than in M2. Ventral to A24b, the cingulate cortex is marked by the presence of two thin bands near the surface, which fade out near the junction with Area 25 (A25). The A25 cortical area is relatively featureless, and generally less dark than A24a above.

Fig. 3b is a section through the anterior commissure. The isocortex here is dominated by the large area occupied the somatosensory cortex (S1Br, S1FL and S1HL, and S2), with the motor and cingulate areas dorsomedially and the insular cortex ventrally. In this section, we have identified, in ventrodorsal order, the piriform cortex (Pir), the insular cortical areas (Ins), the secondary somatosensory cortex (S2), the barrel field of the primary somatosensory cortex (S1BF), the forelimb and hindlimb regions of the somatosensory cortex (S1FL and S1HL respectively), the primary (M1) and secondary (M2) motor cortex, and the cingulate cortex (A24a and A24b).

The piriform cortex, situated ventrolaterally, has a thin dark band in layer 2 surmounted superficially by a light band, which occupies deep half of layer 1. The dark band fades out at the dorsal end of the piriform cortex, signaling the beginning of the insular cortex. Layer 3 of the piriform cortex is of medium intensity, which ends at the beginning of the insular cortex. The ventral boundary of the piriform cortex is clearly marked by the darkening of layer 2 of the cortical–amygdala transition zone (CxA).

The insular cortex is very pale and the boundary with S1 is easy to define. The boundary with the piriform cortex is not as clear, but the end of the dark piriform layer 2 is usually a good guide.

The S2 cortex is much darker overall than the insular cortex, and dark bands in layers 2/3 and layers 5/6 are prominent. Overall, S2 appears darker than S1, especially in layer 6. Layer 2 sometimes shows a characteristic alternation of dark and light bands that is not seen in S1BF.

Within S1, a superficial dark band (in layers 2 and 3) is separated from a deep dark band (layer 5) by a distinct light band. This light band appears to include layer 4 and the outer part of layer 5. There is a third dark band in the deep part of layer 6, but this is not as wide as that seen in S2. Within S1, there is a distinct subdivision into the ventrally placed S1BF and the more dorsal limb areas (S1FL and S1HL). The limb areas are marked by much greater intensity in layers 2 and 3, and slightly greater intensity in the deep dark band (layer 5).

At the junction of S1 and M1, the outer dark band becomes much thinner in the motor cortex, and the middle light band (layers 4 and outer 5) becomes less distinct, and is mostly filled in with small dark patches. The overall greater intensity in layers 2 to 6 in M1 distinguishes it from M2. The superficial dark band becomes much thinner in M2, but appears darker than in M1. The dark band becomes a very thin line at the junction of M2 and the cingulate cortex (A24b), and almost disappears at the junction of A24b and A24a.

Fig. 3c is a section through the caudal part of the barrel field of the somatosensory cortex. It shows the parietal association areas lying between the S1 trunk area and the retrosplenial cortex. It also shows the rostral part of the ectorhinal and perirhinal cortical areas between S2 and the piriform cortex. The most striking features of this section are the bright bands in the deep layers of Area 30 of the cingulate cortex (A30) and the two dark bands in the primary somatosensory cortex (S1Tr and S1BF). Between A30 and S1Tr is a mostly pale area, representing the parietal association cortex. The medial parietal association cortex (MPtA) is pale throughout but the adjacent lateral parietal association cortex (LPtA) is darker in the two major dark bands, but not as hypointense as S1Tr. S1Tr has a very prominent thick superficial dark band and there is a suggestion of a lighter staining dysgranular zone at the lateral margin where it abuts the S1 barrel field (S1BF). The superficial and deep hypointense bands in S1BF are very obvious and there is in places a suggestion of patches in the intervening lighter layer, which may represent barrels in layer 4. At the ventrolateral margin of S1BF there is an abrupt decrease in the thickness and relative intensity of the dark bands, so that they appear less dark and more diffuse in S2. Ventral to S2 the dark layers become even lighter and merge in the region of the ventral auditory association cortex (AuV). Ventral to AuV the dark bands become less prominent as you progress to the region of the ectorhinal cortex (Ect). The perirhinal cortex (PRh), is ventral to Ect and marked by a dark patch in the deepest layers, in contrast to the lack of dark patch in the deeper layers of Ect. The border between PRh and the piriform cortex is not easy to define. The best guide is the appearance of a bright superficial layer in the piriform cortex, and the decrease in intensity of the deep patch of density in PRh. Returning to the dorsomedial cortex, it should be noted that the transition from A30 to A29c is marked by a loss of the superficial dark band that characterizes A30.

Fig. 3d is a section, through the splenium (caudal end) of the corpus callosum and the caudal tip of S1. It shows the primary visual

Please cite this article as: Ullmann, J.F.P., et al., A segmentation protocol and MRI atlas of the C57BL/6J mouse neocortex, NeuroImage (2013), http://dx.doi.org/10.1016/j.neuroimage.2013.04.008

cortex (V1), the primary auditory cortex (Au1) and their respective association areas. From a functional point of view, this sections cuts through the primary visual cortex (V1), the primary auditory cortex (Au1) and the rostral portion of the entorhinal cortex (Ent). In terms of the MR image, the dominant features are a dark superficial band across the primary (V1) and secondary (V2) visual cortical

Table 1
Neocortical segmentation in coronal sections using T_2^*-weighted images. For each structure the name and abbreviation is listed according to Paxinos and Franklin and the Allen Brain Reference Atlas, a color code for the region, an average volume, and an average signal intensity as a percent of the maximum.

Region	The mouse brain in stereotaxic coordinates: Structure names	The mouse brain in stereotaxic coordinates: Abbreviations	The allen reference atlas: Abbreviations	The allen reference atlas: Structure names	Average volume (mm^3)	Average signal intensity (%)
Pallium						
Medial pallium						
Subicular complex						
	Presubiculum	PrS	PRE	Presubiculum	0.27	70.04
	Parasubiculum	PaS	PAR	Parasubiculum	1.42	70.07
	Dorsal subiculum	DS	SUBd	Subiculum, dorsal part	0.74	68.04
	Postsubiculum	Post	POST	Postsubiculum	0.64	69.17
	Subiculum transition area	STr	SUBv	Subiculum, ventral part	2.08	67.83
Entorhinal cortex						
	Medial entorhinal cortex	MEnt	ENTm, ENTmv	Entorhinal area, medialpart, ventral zone	0.58	70.65
	Caudomedial entorhinal cortex	CEnt	ENTm	Entorhinal area, medial part, dorsal zone	4.84	67.93
	Dorsal intermediate entorhinal cortex	DIEnt	ENTl	Entorhinal area, lateral part	1.67	69.16
	Dorsolateral entorhinal cortex	DLEnt	ENTl	Entorhinal area, lateral part	3.11	69.46
	Ventral intermediate entorhinal cortex	VIEnt	ENTl	Entorhinal area, lateral part	0.87	70.21
	Dorsal tenia tecta	DTT	TTd	Tenia tecta, dorsal part	0.84	72.69
	Ventral tenia tecta	VTT	TTv	Tenia tecta, ventral part	0.15	72.55
Dorsal pallium						
Frontal region						
	Dorsolateral orbital cortex	DLO	AId	Agranular insular area, dorsal part	0.55	68.47
	Frontal cortex, area 3	Fr3	MOp	Primary motor area	0.65	68.59
	Frontal association cortex	FrA	FRP	Frontal pole, cerebral cortex	4.54	68.46
	Lateral orbital cortex	LO	ORBl	Orbital area, lateral part	2.44	67.78
	Primary motor cortex	M1	MOp	Primary motor area	6.68	68.00
	Secondary motor cortex	M2	MOs	Secondary Motor area	6.52	69.09
	Medial orbital cortex	MO	ORBm	Orbital area, medial part	1.37	70.99
	Ventral orbital cortex	VO	ORBvl	Orbital area, ventrolateral part	1.16	68.95
Parietal region						
	Lateral parietal association cortex	LPtA	PTLp	Posterior parietal association areas	0.30	69.22
	Medial parietal association cortex	MPtA	PTLp	Posterior parietal association areas	0.46	69.50
	Parietal cortex, posterior area, rostral part	PtPR	PTLp	Posterior parietal association areas	0.12	68.86
	Somatosensory cortex					
	Primary somatosensory cortex	S1	SSp	Primary somatosensory area	3.82	68.58
	Primary somatosensory cortex, barrel field	S1BF	SSp-bfd	Primary somatosensory cortex, barrel field	9.11	68.41
	Primary somatosensory cortex, dysgranular zone	S1DZ	SSp-tr	Primary somatosensory area, trunk	0.38	68.80
	Primary somatosensory cortex, forelimb region	S1FL	SSp-ul	Primary somatosensory area, upper limb	3.96	68.10
	Primary somatosensory cortex, hindlimb region	S1HL	SSp-ll	Primary somatosensory area, lower limb	2.79	68.53
	Primary somatosensory cortex, jaw region	S1J	SSp-m	Primary somatosensory area, mouth	0.51	68.37
	Primary somatosensory cortex, shoulder region	S1Sh	SSp-tr	Primary somatosensory area, trunk	0.24	68.61
	Primary somatosensory cortex, trunk region	S1Tr	SSp-tr	Primary somatosensory area, trunk	0.71	68.93
	Primary somatosensory cortex, upper lip region	S1ULp	SSp-n	Primary somatosensory area, nose	4.58	68.91
	Secondary somatosensory cortex	S2	SSs	Supplemental somatosensory area	6.11	69.12
Temporal region						
	Auditory cortex					
	Primary auditory cortex	Au1	AUDp	Primary auditory area	1.59	69.26
	Secondary auditory cortex, dorsal area	AuD	AUDd	Dorsal auditory area	1.75	69.97
	Secondary auditory cortex, ventral area	AuV	AUDv	Ventral auditory area	1.74	69.12
	Temporal association area	TeA	TEa	Temporal association areas	2.84	70.63
Occipital region						
	Visual cortex					
	Primary visual cortex	V1	VISp	Primary visual area	2.63	70.29
	Primary visual cortex, binocular area	V1B	VISl	Lateral visual area	2.35	69.61
	Primary visual cortex, monocular area	V1M	VISpm	Posteromedial visual area	2.16	68.66
	Secondary visual cortex, lateral area	V2L	VISal	Anterolateral visual area	3.02	70.25
	Secondary visual cortex, mediolateral area	V2ML	VISam	Anteromedial visual area	1.13	68.78
	Secondary visual cortex, mediomedial area	V2MM	PTLp	Posterior parietal association areas	1.93	69.19
Cingulate region						
	Cingulate cortex, area 24a	A24a	ACAv	Anterior cingulate area, ventral part	1.67	73.18
	Cingulate cortex, area 24a'	A24a'		Not differentiated	0.62	70.77
	Cingulate cortex, area 24b	A24b	ACAd	Anterior cingulate area, dorsal part	1.63	71.11
	Cingulate cortex, area 24b'	A24b'		Not differentiated	0.59	69.64
	Cingulate cortex, area 25	A25	ILA	Infralimbic area	0.38	72.92
	Cingulate cortex, area 29a	A29a	RSPv	Retrosplenial area, ventral part	0.57	70.71
	Cingulate cortex, area 29b	A29b	RSPv	Retrosplenial area, ventral part	0.45	72.55
	Cingulate cortex, area 29c	A29c	RSPv	Retrosplenial area, ventral part	1.76	68.82
	Cingulate cortex, area 30	A30	RSPd	Retrosplenial area, dorsal part	2.95	68.78
	Cingulate cortex, area 32	A32	PL	Prelimbic area	1.67	71.52
Insular region						
	Insular region, not subdivided	Ins		Not differentiated	6.55	71.14
	Ectorhinal cortex	Ect	ECT	Ectorhinal area	2.85	69.96
	Perirhinal cortex	PRh	PERI	Perirhinal area	2.45	69.28

Please cite this article as: Ullmann, J.F.P., et al., A segmentation protocol and MRI atlas of the C57BL/6J mouse neocortex, NeuroImage (2013), http://dx.doi.org/10.1016/j.neuroimage.2013.04.008

Table 1 (*continued*)

Region	The mouse brain in stereotaxic coordinates: Structure names	Abbreviations	The allen reference atlas: Abbreviations	Structure names	Average volume (mm^3)	Average signal intensity (%)
Lateral pallium						
Insular claustrum						
Claustrum		Cl	CLA	Claustrum	0.20	67.96
Claustrum, dorsal part		DCl	CLA	Claustrum	0.21	72.07
Claustrum, ventral part		VCl	CLA	Claustrum	0.45	73.10
Ventral pallium						
Endopiriform claustrum						
Dorsal nucleus of the endopiriform		DEn	EPd	Endopiriform nucleus, dorsal part	1.06	70.13
Intermediate nucleus of the endopiriform claustrum		IEn		Not differentiated	0.43	66.51
Ventral nucleus of the endopiriform claustrum		VEn	EPv	Endopiriform nucleus, ventral part	0.37	70.23
Piriform cortex area						
Cortex-amygdala transition zones		CxA	PIR	Piriform area	0.69	66.07
Piriform cortex		Pir	PIR	Piriform area	8.92	71.15
Amygdalopiriform transition area		APir	TR	Postpiriform transition area	0.83	69.64
Rostral amygdalopiriform area		RAPir	PAA	Piriform-amygdalar area	0.34	67.48
Posterolateral cortical amygdaloid area		PLCo	COApl	Cortical amygdalar area, posterior part, lateral zone	0.75	67.67
Posteromedial cortical amygdaloid area		PMCo	COApm	Cortical amygdalar area, posterior part, medial zone	1.08	70.20
Fiber Groups						
Corpus callosum / External capsule		cc/ec	cc/ec	Corpus callosum / External capsule	6.63	50.60
Cingulum		cg	cing	Cingulum bundle	0.67	53.43
Dorsal fornix		df	df	Dorsal fornix	0.03	41.97
Dorsal hippocampal fissure		dhc	dhc	Dorsal hippocampal fissure	1.06	53.63
Forceps minor of the corpus callosum		fmi	fa	Corpus callosum, anterior forceps	1.23	57.34
Lateral olfactory tract		lo	lot	Lateral olfactory tract	0.29	43.33

areas and an intensely dark patch in the area of the ventral auditory association cortex (AuV). Within the visual region, V1 can be distinguished from the lateral and medial visual association areas (V2L, V2ML, and V2MM) on account of the intensification in the superficial dark band in V1. Between V2L and the dark patch marking AuV is a lighter area that includes, from dorsal to ventral, a small caudal part of S1, the dorsal auditory association area (AuD), and the primary auditory cortex (Au1).

The area between the dark patch of AuV and the piriform cortex includes four areas that are difficult to separate. From dorsal to ventral, they are the temporal association areas (TeA), the ectorhinal cortex (Ect), the perirhinal cortex (PRh), and the rostral tip of the entorhinal cortex (DLEnt). It should be noted that the designated location of PRh in the Paxinos and Franklin atlas (Paxinos and Franklin, 2013) is inaccurate, since the PRh in the mouse, sits on the upper bank of the rhinal fissure and not the lower bank (Witter, 2012).

Fig. 3e is a section through the caudal tip of the dentate gyrus. It shows the center of primary visual cortex (V1M and V1B), with visual association areas on either side of the primary auditory cortex (Au1), together with their respective association areas. The most striking features of this section are at the dorsomedial corner, where the very pale retrosplenial cortex abuts three distinct hypointense bands in the mediomedial area of the secondary visual cortex (V2MM). The darkest of these bands is in layer 3, and the two others are in superficial layer 5 and at the layers 1–2 border. V2MM is hard to distinguish from the mediolateral area of the secondary visual cortex (V2ML), but the layer 3 band is usually darker in V2MM. The area occupied by the primary visual cortex (V1M and V1B) is in general lighter than the medial areas of the secondary visual cortex above and the lateral area of the secondary visual cortex (V2L) below. The monocular part of V1 (V1M) has more distinct hypointense bands on either side of layer 4 than seen in the binocular part (V1B). The dark bands in V2L are thicker and more blurred than in medial areas of the secondary visual cortex and V1M. There is an abrupt change from the dark bands in V2L to the lighter TeA area below it. The ectorhinal cortex (Ect) ventral to the temporal association areas (TeA) is lighter still. Below Ect is a dark patch just dorsal to the rhinal fissure, marking the perirhinal cortex (PRh).

Three-dimensional reconstructions

Fig. 4 shows three-dimensional reconstructions of the C57BL/6J neocortex from a dorsal and lateral perspective. Comparisons with

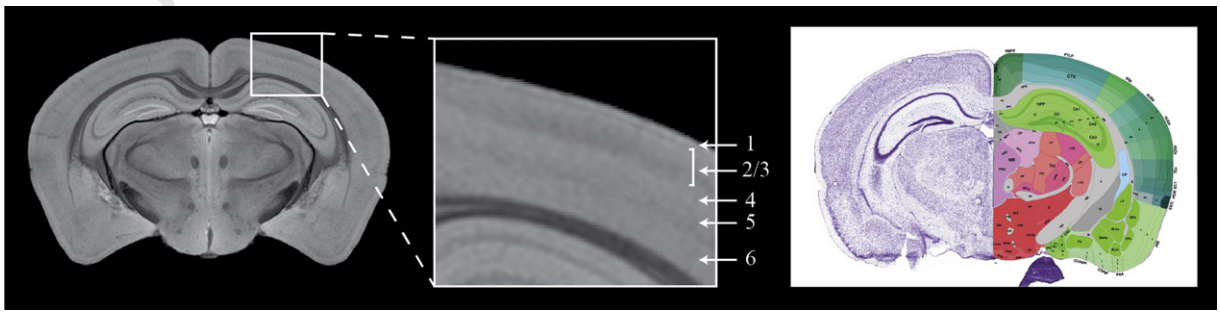

Q2 **Fig. 2.** Lamination of the neocortex on the MRI minimum deformation model. While the six layers could be identified, segmentation of the layers was not performed, as it was difficult to distinguish the layers across the entire cortex. For reference a corresponding section was taken from The Allen Reference Atlas (http://www.mouse.brain-map.org/static/atlas. Note that the designation of the areas in this location does not match the Paxinos & Franklin Atlas (2013).

Please cite this article as: Ullmann, J.F.P., et al., A segmentation protocol and MRI atlas of the C57BL/6J mouse neocortex, NeuroImage (2013), http://dx.doi.org/10.1016/j.neuroimage.2013.04.008

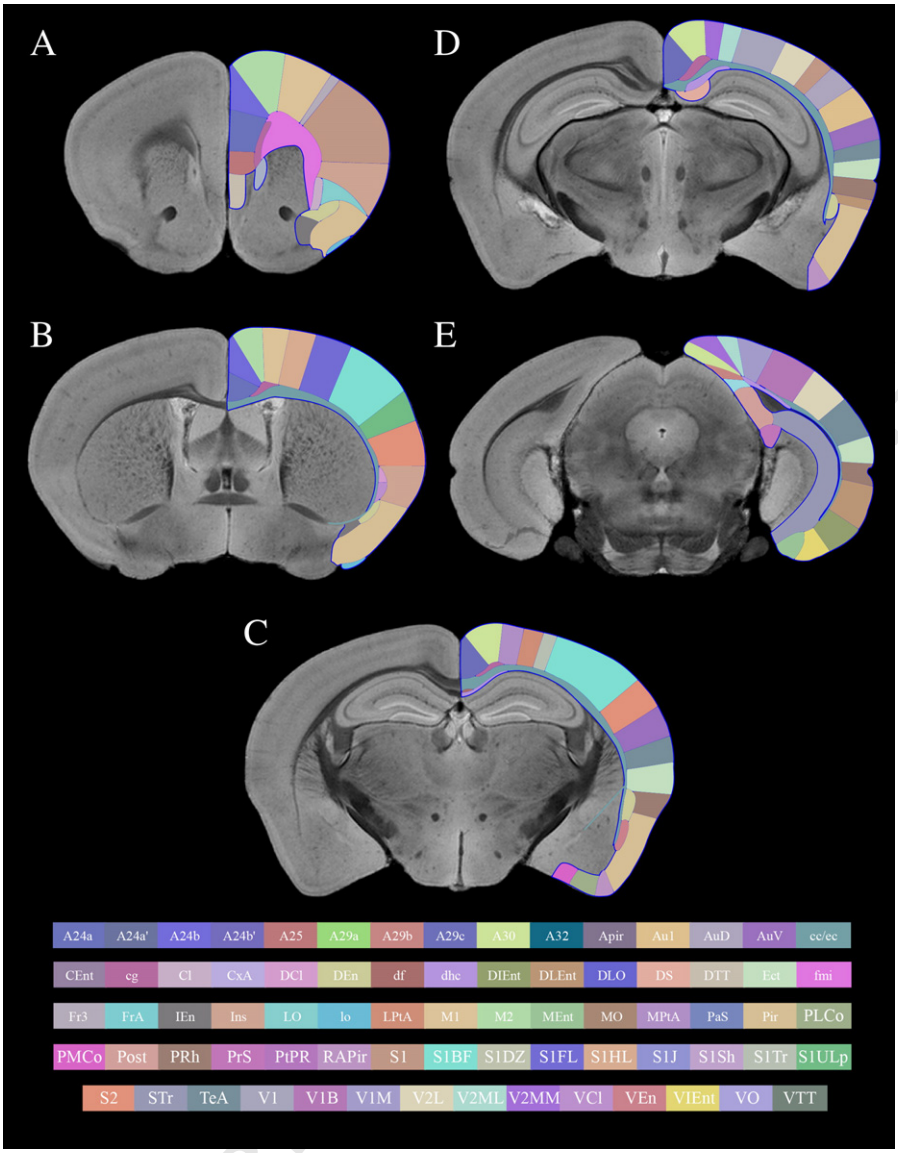

Fig. 3. Segmentation of the C57BL/6J neocortex. Representative T_2* minimum deformation images. Full structure names can be found in Table 1.

other MRI-based atlases were difficult due to the limited segmentation done by previous studies, however our total neocortical volume (134.80 mm^3) is similar to previous studies (see Table 2). From a visual perspective our surface renderings are also comparable with the three-dimensional drawings done by Kirkcaldie (2012) which incorporated information from a range of sources. However it differs

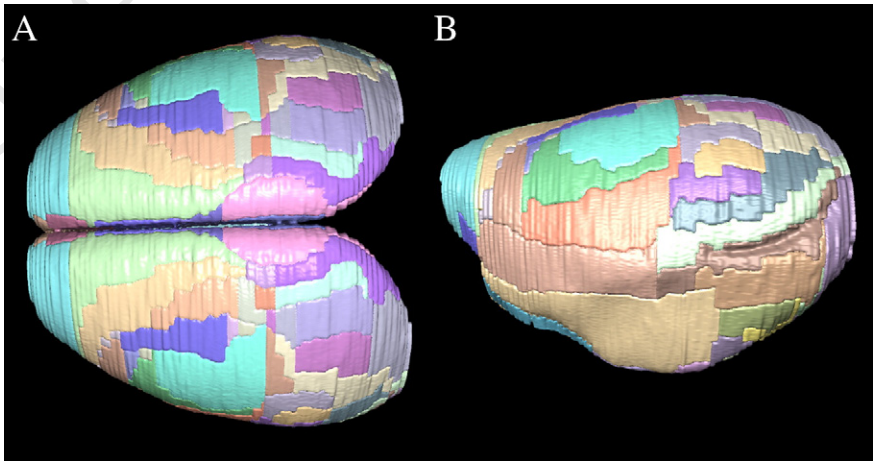

Fig. 4. Three-dimensional surface renderings of the C57BL/6J mouse neocortex. The color code for all segmented regions is shown in Table 1.

Please cite this article as: Ullmann, J.F.P., et al., A segmentation protocol and MRI atlas of the C57BL/6J mouse neocortex, NeuroImage (2013), http://dx.doi.org/10.1016/j.neuroimage.2013.04.008

Table 2
C57BL/6J neocortical volume.

	Age/sex (weeks, M/F)	Resolution (μm^3)	Average volume (mm^3)
Ma et al. (2005), ($n = 10$)	12–14, M	47	144.9 ± 6.0
Ali et al. (2005), ($n = 6$)	9, M	90	No info
MacKenzie-Graham et al. (2006), ($n = 11$)	6–8, F	60	141.2 ± 1.3
Sharief et al. (2008), ($n = 6$)	9, M	43	No info
Badea et al. (2007), ($n = 6$)	9, M	43	~180 ± 10.0
Dorr et al. (2008), ($n = 20$)	12, M	32	134.6 ± 3.6[a]
Johnson et al. (2010), ($n = 14$)	9–11, M	21.5	184.36
Present study, ($n = 18$)	12, M	15	134.80[b]

[a] Note that this volume includes only the entorhinal area, frontal, occipital and parieto-temporal lobes.
[b] Note that this volume does not include the fiber groups listed in Table 1.

from The Allen Reference Atlas desktop application (used in Brain Explorer) (Lau et al., 2008a), as it uses 8 week-old mice and a different ontology and segmentation methodology.

Discussion

We have developed a segmentation protocol for the mouse neocortex with operational criteria based upon signal intensity in T_2*-weighted high-resolution magnetic resonance scans. Employing our methodology, we then segmented a minimum deformation model of the C57BL/6J mouse brain (Janke et al., 2012) to create an atlas of the neocortex consisting of 74 structures. This is a substantially greater number of structures than in previous MRI-based atlases, which either left the cortex as one structure (Badea et al., 2007; Johnson et al., 2010) or parcellated the neocortex into four major regions (Dorr et al., 2008). In addition, to facilitate use of the atlas and enhance the existing framework for multi-modal mapping of the mouse brain (Hawrylycz et al., 2011) we have placed the isocortex atlas in Waxholm space (Johnson et al., 2010). This combined process has brought about two issues that need to be considered: 1) MRI contrast, image registration, and minimum deformation atlas creation; and 2) ontological and segmentation issues associated with the array of mouse brain atlases.

Contrast, registration and atlases

In this study we used Magnevist®, a gadolinium-based contrast agent, which altered relaxation times, in order to enhance contrast between gray and white matter regions (Johnson et al., 2002; Ullmann et al., 2010). Differences in intensity were crucial to differentiating between cortical regions. Magnevist® is a paramagnetic contrast agent that possesses one or two open coordination sites for protons that when bound result in a reduced hydrogen-proton relaxation time (Weinmann et al., 1984). In brain tissue, where the majority of hydrogen protons are present in water molecules, Magnevist® is most likely to be found where water is present. Hence, Magnevist® further increases T_2* signal intensity in structures that have a high density of large neurons and a large water content compared with structures that have low water content such as fiber tracts.

The neocortical lamination shown in Fig. 2 provides an example of the correlation of Magnevist® and cytoarchitectonics. While relatively uniform cytoarchitectonically, the neocortex possesses glia, a range of neuron types, and a huge number of axons and dendrites (Kirkcaldie, 2012) allowing us to match alternating dark and light bands of image intensity to corresponding changes in neuronal density and myelination. For example, Layer (a) is hyperintense as it corresponds to the external plexiform Layer I, which contains few neurons (Peters and Jones, 1984). In contrast Layer (d), is hypointense due to the population of large pyramidal neurons and their axons found in Layer V (Kirkcaldie, 2012). The relationship we found between the MRI relative intensity and the cytoarchitectonics is similar to the results achieved by previous studies, which used specific imaging sequences to enhance visualization of the cortical layers (Barazany and Assaf, 2012; Boretius et al., 2009). Because of the enhancement in contrast with Magnevist® and the increased resolution achieved via registration and creation of a minimum deformation atlas, special sequences were not required to identify differences between cortical regions in our study. It is possible that the combination of new sequences with our methods will allow even finer distinctions between cortical regions to be made.

Minimum deformation atlas modeling provided a number of benefits for characterizing neocortical regions. When compared with images from an individual mouse, the average model exhibited a greater signal to noise ratio. In general, the increase in signal to noise ratio is proportional to the number of data sets used to generate the model. The creation of a minimum deformation atlas results in a down-weighting of artifacts present on a single image, and so further reduces noise. Finally, the creation of a minimum deformation atlas allowed us to create a map of anatomical structures that was closer to that of the population than an atlas based on an individual brain. Neocortical structures segmented on the average model represent the average morphology (size and shape) of a structure and the average signal intensity.

Translating our model to an in vivo MRI data set is critically dependent on the accuracy of registration to the atlas. In vivo imaging does not have the same range of intensity differences between sub-regions that is generated in our ex vivo imaging data from the use of Magnevist® as a contrast agent. This makes registration between our MRI model and an in vivo data set challenging as only major internal and external landmarks can be used. As a result, careful assessment of the registration will be necessary to validate its accuracy. Important future research includes new acquisition techniques to overcome this obstacle.

Ontological and segmentation differences between the Paxinos/Franklin mouse brain atlas (PFA) and the Allen Reference Atlas (ARA)

This neocortical atlas has been placed into Waxholm space to facilitate correlations within an existing framework for multi-modal mapping of the mouse brain (Hawrylycz et al., 2011). We note, however, that there are differences in nomenclature and segmentation boundaries between PFA and the ABA, the two most widely cited mouse brain atlases, making direct comparisons difficult for some structures. In Table 1, we provide the corresponding names and abbreviations for both atlases. The principal differences can be grouped into the following categories. Firstly, there are different abbreviations of the name for a single structure. For example, the primary auditory cortex is abbreviated Au1 in the PFA and AUDp in the ABA, and the secondary motor area is labeled M2 in the PFA and MOs in the ABA. Secondly, for some structures, segmentation into more detailed sub-structures has been performed in one atlas but not the other. The somatosensory and retrosplenial regions are more finely subdivided in the PFA, and the auditory regions are subdivided into smaller regions in the ABA. Thirdly, for a small number of structures, the two atlases do not show concordant boundaries. For example, the visual cortex does not begin in the ABA until the beginning of the dorsal hippocampal commissure (dhc) while in the PFA, it starts at the caudal end of the corpus callosum. The secondary motor area begins more rostrally in the ABA than in the PFA. In light of these differences, we advise care when using both atlases in combination and we suggest that future studies clearly state which atlas was used as a reference. In future, incorporation of ontologies based on gene expression data into multi-modal atlases may allow clearer delineations and resolve some of these disparities.

Conclusion

We provide detailed guidelines for segmenting the isocortex on magnetic resonance images of the C57BL/6J mouse brain as well as mean volumes and relative image intensities. To facilitate its use, the minimum deformation atlas and two hierarchical label fields one with

Please cite this article as: Ullmann, J.F.P., et al., A segmentation protocol and MRI atlas of the C57BL/6J mouse neocortex, NeuroImage (2013), http://dx.doi.org/10.1016/j.neuroimage.2013.04.008

only major structural regions segmented and one containing the individual regions are available in a variety of imaging formats for download at http://www.imaging.org.au/AMBMC/Cortex. By following our image acquisition protocol, future studies can register our atlas to their data to perform automatic segmentation of the isocortex. The atlas will also aid the investigation of neocortical changes in novel mouse strains based on C57BL/6J background.

Funding

This work was supported by the National Health and Medical Research Council (NHMRC) of Australia (grant no. 436673) and a National Computational Infrastructure Grant (grant dc0). We would like to thank the National Imaging Facility (NIF) and the Queensland NMR Network (QNN) for access to the 16.4 T scanner and technical support. In addition, we would like to thank Dr. Marianne Keller and the other members of AMBMC.

References

Airey, D.C., Robbins, A.I., Enzinger, K.M., Wu, F., Collins, C.E., 2005. Variation in the cortical area map of C57BL/6J and DBA/2J inbred mice predicts strain identity. BMC Neurosci. 6 (Article No.: 18).

Airey, D.C., Wu, F., Guan, M., Collins, C.E., 2006. Geometric morphometrics defines shape differences in the cortical area map of C57BL/6J and DBA/2J inbred mice. BMC Neurosci. 7 (Article No.: 7).

Ali, A.A., Dale, A.M., Badea, A., Johnson, G.A., 2005. Automated segmentation of neuroanatomical structures in multispectral MR microscopy of the mouse brain. Neuroimage 27, 425–435.

Badea, A., Ali-Sharief, A.A., Johnson, G.A., 2007. Morphometric analysis of the C57BL/6J mouse brain. Neuroimage 37, 683–693.

Barazany, D., Assaf, Y., 2012. Visualization of cortical lamination patterns with magnetic resonance imaging. Cereb. Cortex 22, 2016–2023.

Benveniste, H., Ma, Y., Dhawan, J., Gifford, A., Smith, S.D., Feinstein, I., Du, C., Grant, S.C., Hof, P.R., 2007. Anatomical and functional phenotyping of mice models of Alzheimer's disease by MR microscopy. Ann. N. Y. Acad. Sci. 1097, 12–29.

Bohland, J.W., Bokil, H., Pathak, S.D., Lee, C.-K., Ng, L., Lau, C., Kuan, C., Hawrylycz, M., Mitra, P.P., 2010. Clustering of spatial gene expression patterns in the mouse brain and comparison with classical neuroanatomy. Methods (Amsterdam) 50, 105–112.

Boretius, S., Kasper, L., Tammer, R., Michaelis, T., Frahm, J., 2009. MRI of cellular layers in mouse brain *in vivo*. Neuroimage 47, 1252–1260.

Caviness Jr., V.S., 1975. Architectonic map of neocortex of the normal mouse. J. Comp. Neurol. 164, 247–263.

Dong, H.W., 2008. The Allen Reference Atlas: A Digital Color Brain Atlas of the C57BL/6J Male Mouse. John Wiley & Sons Inc., Hoboken, NJ, US.

Dorr, A.E., Lerch, J.P., Spring, S., Kabani, N., Henkelman, R.M., 2008. High resolution three-dimensional brain atlas using an average magnetic resonance image of 40 adult C57BL/6J mice. Neuroimage 42, 60–69.

Fonov, V., Evans, A.C., Botteron, K., Almli, C.R., McKinstry, R.C., Collins, D.L., 2011. Unbiased average age-appropriate atlases for pediatric studies. Neuroimage 54, 313–327.

Franklin, K., Paxinos, G., 2008. The Mouse Brain in Stereotaxic Coordinates, 3rd ed. Academic Press, San Diego.

Gaglani, S.M., Lu, L., Williams, R.W., Rosen, G.D., 2009. The genetic control of neocortex volume and covariation with neocortical gene expression in mice. BMC Neurosci. 10, 44.

Hawrylycz, M., Bernard, A., Lau, C., Sunkin, S.M., Chakravarty, M.M., Lein, E.S., Jones, A.R., Ng, L., 2010. Areal and laminar differentiation in the mouse neocortex using large scale gene expression data. Methods (Amsterdam) 50, 113–121.

Hawrylycz, M., Baldock, R.A., Burger, A., Hashikawa, T., Johnson, G.A., Martone, M., Ng, L., Lau, C., Larsen, S.D., Nissanov, J., Puelles, L., Ruffins, S., Verbeek, F., Zaslavsky, I., Boline, J., 2011. Digital atlasing and standardization in the mouse brain. PLoS Comput. Biol. 7, e1001065.

Hof, P.R., Young, W.G., Bloom, F.E., Belichenko, P.V., Celio, M.R., 2000. Comparative Cytoarchitectonic Atlas of the C57BL/6 and 129/Sv Mouse Brains. Elsevier Academic Press, Amsterdam.

Jan, T.A., Lu, L., Li, C.-X., Williams, R.W., Waters, R.S., 2008. Genetic analysis of posterior medial barrel subfield (PMBSF) size in somatosensory cortex (SI) in recombinant inbred strains of mice. BMC Neurosci. 9 (Article No.: 3).

Janke, A.L., Ullmann, J.F.P., Kurniawan, N.D., Paxinos, G., Keller, M., Yang, Z., Richards, K., Egan, G., Petrou, S., Galloway, G., Reutens, D., 2012. 15 μm average mouse models in Waxholm space from 16.4 T 30 μm images. 20th Annual ISMRM Scientific Meeting and Exhibition, Melbourne, Australia.

Johnson, G.A., Cofer, G.P., Gewalt, S.L., Hedlund, L.W., 2002. Morphologic phenotyping with MR microscopy: the visible mouse. Radiology 222, 789–793.

Johnson, G.A., Badea, A., Brandenburg, J., Cofer, G., Fubara, B., Liu, S., Nissanov, J., 2010. Waxholm space: an image-based reference for coordinating mouse brain research. Neuroimage 53, 365–372.

Jones, E.g., 2007. The Thalamus. Cambridge University Press, Cambridge.

Kirkcaldie, M.T., 2012. Neocortex. In: Watson, C., Paxinos, G., Puelles, L. (Eds.), The Mouse Nervous System. Elsevier Academic Press, San Diego, p. 814.

Larsen, D.D., Wickersham, I.R., Callaway, E.M., 2007. Retrograde tracing with recombinant rabies virus reveals correlations between projection targets and dendritic architecture in layer 5 of mouse barrel cortex. Front. Neural Circ. 1, 5.

Lau, J.C., Lerch, J.P., Sled, J.G., Henkelman, R.M., Evans, A.C., Bedell, B.J., 2008a. Longitudinal neuroanatomical changes determined by deformation-based morphometry in a mouse model of Alzheimer's disease. Neuroimage 42, 19–27.

Lau, C., Ng, L., Thompson, C., Pathak, S., Kuan, L., Jones, A., Hawrylycz, M., 2008b. Exploration and visualization of gene expression with neuroanatomy in the adult mouse brain. BMC Bioinformatics 9 (Article No.: 153).

Lerch, J.P., Carroll, J.B., Dorr, A., Spring, S., Evans, A.C., Hayden, M.R., Sled, J.G., Henkelman, R.M., 2008a. Cortical thickness measured from MRI in the YAC128 mouse model of Huntington's disease. Neuroimage 41, 243–251.

Lerch, J.P., Carroll, J.B., Spring, S., Bertram, L.N., Schwab, C., Hayden, M.R., Henkelman, R.M., 2008b. Automated deformation analysis in the YAC128 Huntington disease mouse model. Neuroimage 39, 32–39.

Li, C.X., Wei, X., Lu, L., Peirce, J.L., Williams, R.W., Waters, R.S., 2005. Genetic analysis of barrel field size in the first somatosensory area (SI) in inbred and recombinant inbred strains of mice. Somatosens. Mot. Res. 22, 141–150.

Ma, Y., Hof, P.R., Grant, S.C., Blackband, S.J., Bennett, R., Slatest, L., McGuigan, M.D., Benveniste, H., 2005. A three-dimensional digital atlas database of the adult C57BL/6J mouse brain by magnetic resonance microscopy. Neuroscience 135, 1203–1215.

MacKenzie-Graham, A., Tinsley, M.R., Shah, K.P., Aguilar, C., Strickland, L.V., Boline, J., Martin, M., Morales, L., Shattuck, D.W., Jacobs, R.E., Voskuhl, R.R., Toga, A.W., 2006. Cerebellar cortical atrophy in experimental autoimmune encephalomyelitis. Neuroimage 32, 1016–1023.

Meltzer, N.E., Ryugo, D.K., 2006. Projections from auditory cortex to cochlear nucleus: a comparative analysis of rat and mouse. Anat. Rec. A Discov. Mol. Cell. Evol. Biol. 288, 397–408.

Ng, L., Bernard, A., Lau, C., Overly, C.C., Dong, H.-W., Kuan, C., Pathak, S., Sunkin, S.M., Dang, C., Bohland, J.W., Bokil, H., Mitra, P.P., Puelles, L., Hohmann, J., Anderson, D.J., Lein, E.S., Jones, A.R., Hawrylycz, M., 2009. An anatomic gene expression atlas of the adult mouse brain. Nat. Neurosci. 12, 356–362.

Nieman, B.J., Bock, N.A., Bishop, J., Chen, X.J., Sled, J.G., Rossan, J., Henkelman, R.M., 2005. Magnetic resonance imaging for detection and analysis of mouse phenotypes. NMR Biomed. 18, 447–468.

Paxinos, G., Franklin, K., 2013. The Mouse Brain in Stereotaxic Coordinates. Academic Press, San Diego.

Paxinos, G., Watson, C., 2007. The Rat Brain in Stereotaxic Coordinates, Sixth ed. Elsevier Academic Press, San Diego.

Paxinos, G., Watson, C., Carrive, P., Kirkcaldie, M.T., Ashwell, K., 2009. Chemoarchitectonic Atlas of the Rat Brain. Elsevier Academic Press, San Diego.

Peters, A., Jones, E., 1984. Cerebral Cortex, Volume 1: Cellular Components of the Cerebral Cortex. Plenum, New York.

Pitiot, A., Pausova, Z., Prior, M., Perrin, J., Loyse, N., Paus, T., 2007. Magnetic resonance imaging as a tool for *in vivo* and *ex vivo* anatomical phenotyping in experimental genetic models. Hum. Brain Mapp. 28, 555–566.

Sawiak, S.J., Wood, N.I., Williams, G.B., Morton, A.J., Carpenter, T.A., 2009. Voxel-based morphometry in the R6/2 transgenic mouse reveals differences between genotypes not seen with manual 2D morphometry. Neurobiol. Dis. 33, 20–27.

Sharief, A.A., Badea, A., Dale, A.M., Johnson, G.A., 2008. Automated segmentation of the actively stained mouse brain using multi-spectral MR microscopy. Neuroimage 39, 136–145.

Tennant, K.A., Adkins, D.L., Donlan, N.A., Asay, A.L., Thomas, N., Kleim, J.A., Jones, T.A., 2011. The organization of the forelimb representation of the C57BL/6 mouse motor cortex as defined by intracortical microstimulation and cytoarchitecture. Cereb. Cortex 21, 865–876.

Ullmann, J.F.P., Cowin, G., Kurniawan, N.D., Collin, S.P., 2010. Magnetic resonance histology of the adult zebrafish brain: optimization of fixation and gadolinium contrast enhancement. NMR Biomed. 23, 341–346.

Watson, C., Paxinos, G., 2010. Chemoarchitectonic Atlas of the Mouse Brain. Elsevier Academic Press, San Diego.

Weinmann, H.-J., Brasch, R.C., Press, W.-R., Wesbey, G.E., 1984. Characteristics of gadolinium-DTPA Complex: a potential NMR contrast agent. Am. J. Roentgenol. 142, 619–624.

Witter, M., 2012. Hippocampus. In: Watson, C., Paxinos, G., Puelles, L. (Eds.), The Mouse Nervous System. Elsevier Academic Press, San Diego, p. 814.

Wree, A., Zilles, K., Schleicher, A., 1983. A quantitative approach to cytoarchitectonics. VIII. The areal pattern of the cortex of the albino mouse. Anat. Embryol. 166, 333–353.

Zhang, J.Y., Peng, Q., Li, Q., Jahanshad, N., Hou, Z.P., Jiang, M.L., Masuda, N., Langbehn, D.R., Miller, M.I., Mori, S., Ross, C.A., Duan, W.Z., 2010. Longitudinal characterization of brain atrophy of a Huntington's disease mouse model by automated morphological analyses of magnetic resonance images. Neuroimage 49, 2340–2351.